doi:10.1016/j.jmb.2006.10.053 J. Mol. Biol. (2007) 365, 752–763

JMB

Available online at www.sciencedirect.com

ScienceDirect

ELSEVIER

Disulfide Bridges in the Mesophilic Triosephosphate Isomerase from *Giardia lamblia* Are Related to Oligomerization and Activity

Horacio Reyes-Vivas[1]*, Adelaida Diaz[1], Jorge Peon[2] Guillermo Mendoza-Hernandez[3], Gloria Hernandez-Alcantara[1] Ignacio De la Mora-De la Mora[1], Sergio Enriquez-Flores[1] Lenin Dominguez-Ramirez[3] and Gabriel Lopez-Velazquez[1]*

[1]*Laboratorio de Bioquimica Genetica, Instituto Nacional de Pediatria, 04530 Mexico, D.F.*

[2]*Instituto de Quimica Universidad Nacional Autonoma de Mexico 04510, Mexico, D.F.*

[3]*Facultad de Medicina Universidad Nacional Autonoma de Mexico 04510, Mexico, D.F.*

**Corresponding authors*

Triosephosphate isomerase from the mesophile *Giardia lamblia* (GlTIM) is the only known TIM with natural disulfide bridges. We previously found that oxidized and reduced thiol states of GlTIM are involved in the interconversion between native dimers and higher oligomeric species, and in the regulation of enzymatic activity. Here, we found that trophozoites and cysts have different oligomeric species of GlTIM and complexes of GlTIM with other proteins. Our data indicate that the internal milieu of *G. lamblia* is favorable for the formation of disulfide bonds. Enzyme mutants of the three most solvent exposed Cys of GlTIM (C202A, C222A, and C228A) were prepared to ascertain their contribution to oligomerization and activity. The data show that the establishment of a disulfide bridge between two C202 of two dimeric GlTIMs accounts for multimerization. In addition, we found that the establishment of an intramonomeric disulfide bond between C222 and C228 abolishes catalysis. Multimerization and inactivation are both reversed by reducing conditions. The 3D structure of the C202A GlTIM was solved at 2.1 Å resolution, showing that the environment of the C202 is prone to hydrophobic interactions. Molecular dynamics of an *in silico* model of GlTIM when the intramonomeric disulfide bond is formed, showed that S216 is displaced 4.6 Å from its original position, causing loss of hydrogen bonds with residues of the active-site loop. This suggests that this change perturb the conformational state that aligns the catalytic center with the substrate, inducing enzyme inactivation.

Keywords: *Giardia*; triosephosphate; disulfide bonds; glycolysis; Dinamic molecular

Introduction

Giardia lamblia is a eukaryotic parasite that causes human giardiasis. An estimated 200 million people have symptomatic human giardiasis, mainly infants who exhibit a failure-to-thrive syndrome.[1] Infection is initiated by ingestion of cysts, followed by excystation and colonization of the small intestine by the trophozoite. It is known that encystation and excystation involve several important changes at the molecular level that could be related to its infective capacity.[2] Although current drugs against giardiasis are effective,[3] they exhibit severe toxic effects in the host.[4] In addition, there is clear evidence for the emergence of strains resistant to currently used drugs.[5] This has led to the search for novel experimental strategies and new targets for antigiardial drug design.[6] In this regard, it is relevant that *G. lamblia* lacks oxidative phosphorylation;[7,8] thus, the main source of ATP is the glycolytic pathway.[7]

Abbreviations used: TIM, triosephosphate isomerase; GlTIM, *Giardia lamblia* TIM; PfTIM, *Plasmodium falciparum* TIM; GAP, D-glyceraldehyde 3-phosphate; DHAP, dihydroxyacetone phosphate; DTNB, 5,5′-dithio-bis (2-nitrobenzoic acid); ASA, accessible surface area; PG, phosphoglycolate.

E-mail addresses of the corresponding authors: glv@salud.gob.mx

The enzymes of this metabolic pathway have been proposed as potential targets for drug design in other parasites.[9–13]

Recently, we characterized a recombinant triosephosphate isomerase (EC 5.3.1.1) from *G. lamblia* (GlTIM).[13] This enzyme catalyzes the interconversion between D-glyceraldehyde 3-phosphate (GAP) and dihydroxyacetone phosphate (DHAP). The functional and structural characteristics of TIM from diverse organisms have been studied extensively.[12,14–30] The enzyme is the prototype of a $(\alpha/\beta)_8$-barrel motif, which is formed by eight central β-strands surrounded by eight α-helices joined by loops. A detailed knowledge of the properties of GlTIM, at molecular and cellular levels, is necessary to develop this enzyme as target for antigiardial drugs.

The enzymes from the thermophilic organisms, *Pyroccoccus woesei* and *Thermoproteus tenax*, are tetramers;[31,32] TIM from *T. tenax* can exist also as a dimer, although only the tetramer is catalytically active.[33] Before it was found that GlTIM exists in both dimeric and oligomeric states, it was assumed that all the enzymes from mesophilic organisms were dimers. Thus, a unique characteristic of GlTIM is that it undergoes interconversion between dimeric and tetrameric species, both of which are active; however, the k_{cat} of the dimer is twofold higher.

G. lamblia uses free cysteine residues instead of the gluthatione system as the main low molecular mass antioxidant.[34,35] Since the parasite acquires Cys from the intestinal environment,[36] this amino acid could be limiting at some stage of its life-cycle. Indeed, it is probable that cysts suffer deprivation of Cys when they are released from the small intestine. This suggests that the internal milieu of *G. lamblia* facilitates the formation of disulfide bonds. Here, we found that trophozoites and cysts have GlTIM in various oligomeric forms joined through disulfide bonds. Finally, the Cys residues involved in the formation of disulfide bonds in GlTIM were identified; besides, the 3D structure of C202A mutant was resolved at 2.1 Å. The crystal structure allowed the characterization of the environment of the Cys residues of the enzyme.

Results

Oligomeric state of cellular GlTIM

G. lamblia is a mesophilic eukaryote whose life-cycle alternates between vegetative trophozoites and dormant cysts. Since the existence of high oligomers of GlTIM may be of physiological significance, we explored the presence of dimers and higher oligomers in trophozoites and cysts. The concentration of cytoplasmic GlTIM from total protein was determined by optical densitometry of the monomer in gels containing sodium dodecyl sulfate (SDS) under reducing conditions, and detected by Western blots using polyclonal antibodies against GlTIM. We found that cysts have 1.7 μg of GlTIM monomer per 1 mg of total protein, while the trophozoites have 4.9 μg of GlTIM monomer per 1 mg of total protein. Under non-reducing conditions in the SDS-containing gels, trophozoites showed a band with a molecular mass that corresponded to a monomer (28 kDa) plus a band that corresponded to the dimer. A band with molecular mass higher than that of a dimer (≈70 kDa) was also observed (Figure 1(a)); in contrast, under reducing conditions in the SDS-containing gels, a single band of 28 kDa was detected. Western blot of the cyst proteins under non-reducing conditions revealed a single band with a molecular mass greater than 200 kDa (Figure 1(a)). Thus, the data indicate that in both cysts and trophozoites there are species of GlTIM with molecular mass greater than that of the dimer.

It is noteworthy that at least one other protein is associated with GlTIM through a disulfide (-S–S-) bridge. The existence of the complex was evidenced by immunoprecipitation of GlTIM from trophozoites extracts under non-reducing conditions, followed by elution of the retained proteins with an acid buffer. Figure 1(b) shows the SDS-PAGE of the eluted proteins in the absence of reducing agents. Four bands were detected with molecular mass of 160 kDa, 70 kDa, 55 kDa and 28 kDa. This method detects bands corresponding to dimer and monomer of GlTIM (55 kDa and 28 kDa, respectively) and the

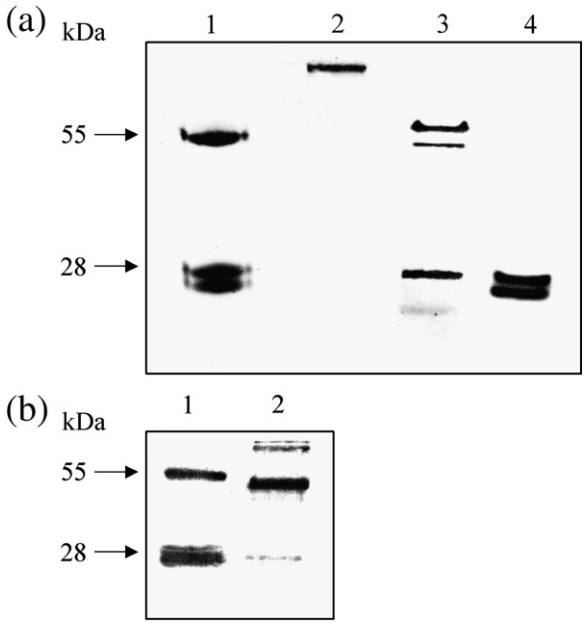

Figure 1. Oligomeric species of cellular GlTIM. (a) Immunodetection of cellular GlTIM by Western blot using anti-GlTIM diluted 1:2500 (v/v). Lane 1, recombinant GlTIM; lane 2, soluble proteins of cysts; lane 3, soluble proteins of trophozoites; lane 4, soluble proteins of trophozoites with DTT. (b) Soluble proteins of trophozoites immunoprecipitated with anti-GlTIM and stained with Coomassie brilliant blue. Lane 1, recombinant GlTIM; lane 2, fractions immunoprecipitaed from proteins of trophozoites.

band of free IgG (160 kDa). These data support the mechanism of multimerization proposed in Figure 5 (see below); the band of 70 kDa might indicate the existence of a complex of GlTIM with another protein.

In situ distribution of GlTIM in trophozoites and cysts

The above data indicate that there are significant differences in the content of GlTIM in trophozoites and cysts. Therefore, we examined if there are differences in the distribution of GlTIM in the two types of cells. The immunofluorescent signal of GlTIM in trophozoites was significantly higher than that observed in cysts (Figure 2(a)). Likewise, the data showed that in the trophozoite, the enzyme is distributed uniformly throughout the cytoplasm, whereas in the cyst, the enzyme is localized preferentially at the periphery of the cell, in close proximity to the cytoplasmic face of the plasma membrane (Figure 2(b)).

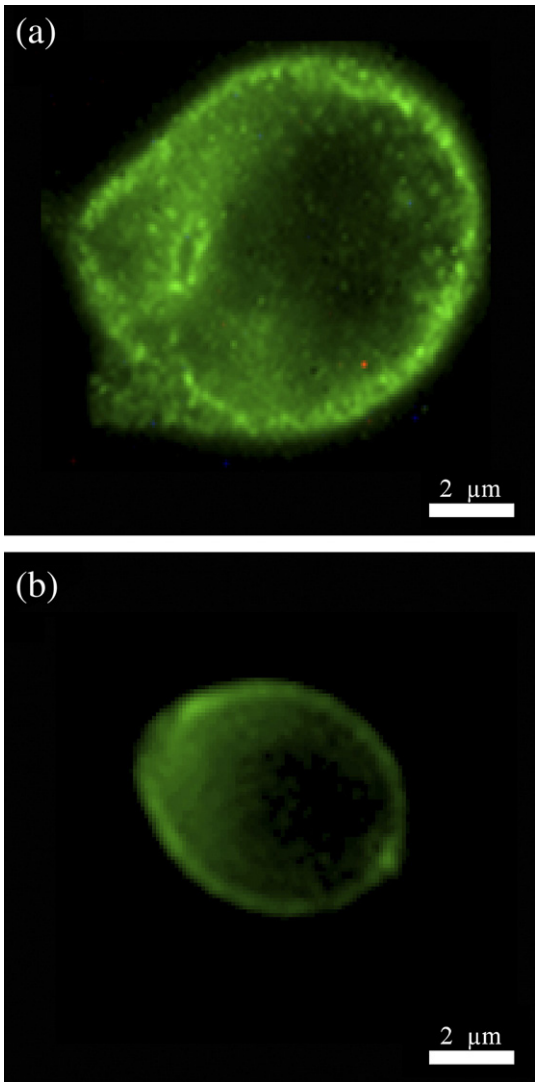

Figure 2. *In situ* distribution of GlTIM. Immunofluorescence image of GlTIM distribution in (a) trophozoites, and (b) cysts. The scale bar represents 2 μm.

Determination of Cys residues involved in the oligomerization of GlTIM

Tetramers of GlTIM are stabilized *via* a disulfide bridge between one of the two monomers of two dimers.[13] This oligomerization suggests that there is an interaction between Cys residues that are localized on the surface of the enzyme. GlTIM contains five Cys residues per monomer (positions 14, 127, 202, 222 and 228). The accessible solvent area (ASA) data and the localization of C202, C222, and C228 (see the crystallographic data below) suggested that they could be involved in the formation of such linkages. On the other hand, residues 14 and 127 are buried in the dimer. Therefore, we prepared the enzyme mutants C202A, C222A and C228A to determine which Cys residues are involved in the formation of the interchain bridges. Size-exclusion chromatography profiles of wild-type GlTIM and the C222A and C228A mutants showed dimeric and tetrameric GlTIMs (Figure 3). After two days of storage, the population of tetramers was enriched with respect to the freshly purified samples. In all cases, the high molecular mass species were transformed to dimers under reducing conditions (Figure 3). In contrast, C202A GlTIM showed only the dimer. We have observed that, even after a year of storage at 4 °C, this mutant failed to form oligomers larger than the dimer.

Crystal Structure of C202A

The overall crystal structure showed the α/β barrel domain characteristic of all TIMs (PDB entry 2DP3). Val instead of Ala in the amino acid sequence was found at position 198, due to a substitution in the PCR process, but this did not affect the kinetic constants of mutant C202A (not shown). All the residues were clearly modeled, with the exception of Thr 257, for which no density was observed. Two sulfate molecules were found at the active site; consequently, loop 6 that is part of the catalytic region was in the closed conformation. In agreement with previous reports, the active-site residues (K13, H95 and E170) are not rigid, showing E170 as the most flexible.[24] The side-chain of E170 observed in the C202A mutant has a value of $\chi^1 = -71°$. This behavior has been reported for the structures of several TIM complexes, in which the catalytic glutamic residues adopt χ^1 values ranging from −29° (PDB entry 1TRD,[37]) to −79° (PDB entry 2YPI)[38] when the catalytic loop is in the closed conformation.

Similar to other TIM crystal structures reported, the dimer interface of the C202A mutant is formed with an important portion of loop 3, which interacts intimately with loop 1 of the other subunit. The residues of loops 1 and 3 provide a significant number of contacts inside the interface. Directed

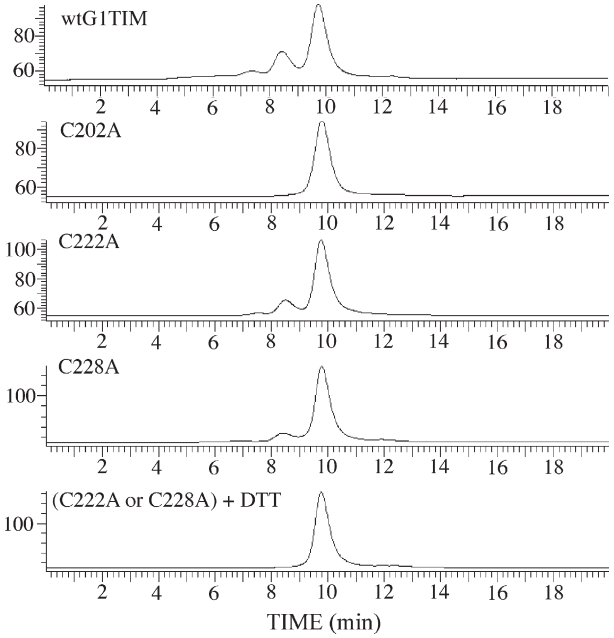

Figure 3. Size-exclusion chromatography of wtGlTIM and single mutants. Gel-filtration elution profiles of wtGlTIM, C202A, C222A, and C228 mutants are shown. For the chromatographic analysis of the enzymes under reducing conditions, the enzymes were first incubated with 1 mM DTT.

mutagenesis of the residues from loop 1 in the TIM of the parasite *Trypanosoma brucei*,[9,39] or deamidation of Asn15 in rabbit TIM,[40] induces a decrease of dimer stability, showing the importance of the interactions of loop 1 with the other subunit. Of the four Cys residues per monomer of the C202A mutant, one of them (C14) occurs at the interface region. The interfacial Cys is present also in the TIM of the parasites *T. brucei, T. cruzi, Leishmania mexicana, Entamoeba histolytica,* and *Plasmodium falciparum*. It has been reported that chemical modification of this residue induces progressive structural alteration and abolition of enzyme activity in those organisms.[11,25,41] Because the corresponding residue in the TIM of mammals is methionine, the interfacial Cys has been established as potential drug target in the aforementioned parasites.

GlTIM contains an intramonomeric disulfide bridge per subunit

In the absence of reducing agents, the k_{cat} value of wild-type (wt)-GlTIM was 2.9(±0.2)×10^5 min^{-1}, and there were three free Cys per monomer (Table 1). When the enzyme was treated with reducing agents, the k_{cat} increased twofold, and the number of Cys that reacted with 5,5′-dithio-bis (2-nitrobenzoic acid) (DTNB) was five per monomer. The k_{cat} and the number of Cys (four per monomer) of the mutants C222A and C228A were markedly similar, with or without reducing agents (Table 1). Hence, the data suggest that C222 and C228 are involved in the formation of an intramonomeric disulfide, and that the formation of this bond decreases enzyme activity by about 50%.

It is important to point out that the k_{cat} of mutants C202A and C228A were 1.6-fold and 2.4-fold lower than that of wt-GlTIM, respectively; thus, the substitution of Cys by Ala in these positions affects the catalytic properties of the enzyme. The k_{cat} of mutant C202A did not show a difference when stored in the absence and in the presence of dithiothreitol (DTT). After six months of storage without reducing agents, the k_{cat} of the enzyme was not modified, albeit the number of free Cys in C202A decreased to three per monomer; which probably results from a spontaneous oxidation process. The data also indicate that, although C202A has residues C222 and C228, it was not able to form the intramonomeric bonds spontaneously.

Formation of the intramonomeric disulfide bond induced by Cu^{2+}

In order to explore the contribution of the intramonomeric disulfide bond to enzyme activity without the participation of intermonomeric disulfides, we examined the effect of Cu^{2+} on the mutant C202A, since it is known that Cu^{2+} promotes the generation of disulfide bonds.[42,43] The addition of copper to C202A GlTIM resulted in the inactivation of the enzyme, and the amount of Cys per subunit dropped to 1.8(±0.06). Treatment of the oxidized enzyme with a reducing agent restored enzyme activity and raised the content of Cys to 4.2(±0.2) per monomer. Similar results were obtained with the wt-GlTIM (not shown).

Table 1. Kinetic constants and free Cys per subunit of mutants and wild-type GlTIM

	K_m (mM)		k_{cat} (10^5 min^{-1})		-SH/monomer	
TIM	Non-reduced	Reduced	Non-reduced	Reduced	Non-reduced	Reduced
wt dimer	0.53±0.03	0.78±0.06	2.9±0.2	4.6±0.16	3.1±0.4	5±0.1
C202A	0.61±0.06	0.8±0.09	2.9±0.1	2.9±0.14	4±0.06	4±0.1
C222A dimer	1.41±0.23	1.8±0.3	5.2±0.26	5±0.4	4±0.25	4±0.8
C222A tetramer	1.4±0.24	n.d.	5.5±0.48	n.d.	3.52±0.06	n.d.
C228A dimer	0.4±0.03	0.25±0.07	1.87±0.2	1.9±0.15	3.83±0.1	4.1±0.03
C228A tetramer	0.27±0.03	n.d.	1.15±0.02	n.d.	3.5±0.1	n.d.

The conditions for determining the kinetics and Cys content are described in Experimental Procedures. The concentration of GAP ranged from 0.5 mM to 3 mM. The values are the averages±standard error of three independent experiments; n.d., not determined.

The effect of Cu^{2+} on the C222A and C228A GlTIMs was studied. The purpose of the experiments was to confirm if indeed an intramonomeric disulfide bond is formed between C222 and C228. The number of Cys per monomer in C222A and C228A GlTIMs decreased to three when the enzymes were treated with Cu^{2+}. However, Cu^{2+} did not induce a decrease in the activity of these mutants. Thus, the overall data with wt-GlTIM and the C202A, C222A, and C228A mutants indicate that inactivation is induced when the intramonomeric disulfide bond between C222 and C228 is established.

The perturbation of catalysis by the disulfide bond formed between the C222 and C228, suggests that there is communication between the region of disulfide and the active site. Therefore, we determined the rate of inactivation of the C202A mutant induced by Cu^{2+} in the presence of the ligand phosphoglycolate (PG),[44] or the substrate GAP in the active site. The rate of inactivation was 35-fold lower with PG than with GAP (tenfold) (Figure 4). This is consistent with the fact that the enzyme affinity for PG ($K_i = 0.07(\pm 0.006)$ mM) is higher than that for GAP ($K_m = 0.53(\pm 0.03)$ mM). Moreover, the number of Cys per monomer in the presence of PG or GAP dropped to 3.2 and 2.5, respectively. Hence, the occupancy of the catalytic site by these ligands diminishes the rate of enzyme inactivation and decreases the rate of formation of the intramolecular disulfide bond.

It is relevant that the formation of the intramolecular disulfide bond under non-reducing conditions decreases enzyme activity by about 50%, whereas the generation of this bond using Cu^{2+} induced the total loss of activity. In this regard, it is relevant to mention that interactions between this metal with other regions of GlTIM might occur, and such a condition must be responsible for the additional inactivation observed in Figure 4. The effect of enzyme inactivation as well as other structural alterations by Cu^{2+} binding has been described for other proteins.[42,45]

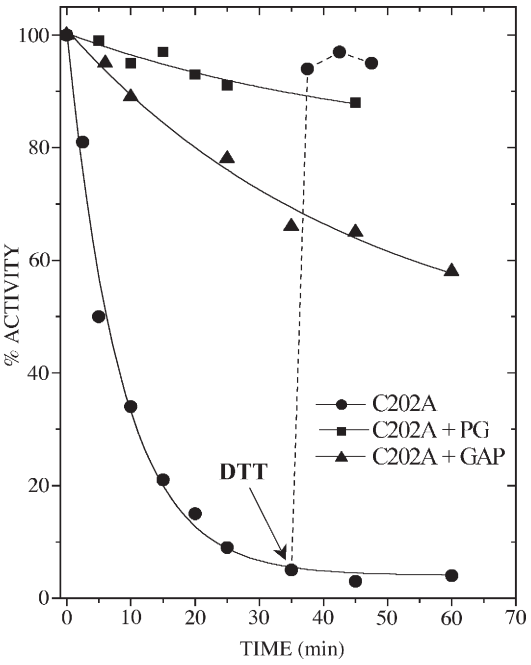

Figure 4. Effect of Cu^{2+} on the activity of C202A incubated without and with ligands. The rates of inactivation of C202A after the incubation with Cu^{2+} in the absence of ligand, or in the presence of GAP or PG are shown. The arrow indicates the time of addition of 1 mM DTT.

Discussion

G. lamblia contains different oligomeric stages of GlTIM

Western blot analysis of trophozoites showed that they possess dimers and higher molecular mass oligomers of GlTIM. We observed a band of about 70 kDa that apparently corresponds to GlTIM linked to another protein by disulfide bonds. In cysts, a band of molecular mass greater than 200 kDa was observed. These data indicate that GlTIM oligomerization is of functional significance in some stage of the life-cycle of *G. lamblia*. The findings illustrate that the intracellular conditions of *G. lamblia* are favorable for the formation of disulfides.

Intermolecular disulfide bridge and oligomerization

GlTIM shows unusual characteristics with respect to the TIMs described so far. We have reported that GlTIM might exist in dimeric, tetrameric, and higher oligomeric states.[13] We show here that the intersubunit bond formed between the C202 of each monomer accounts for oligomerization. This conclusion is based on the observation that even after a year under non-reducing conditions, the C202A mutant failed to form high molecular mass oligomers. On the other hand, higher molecular mass oligomers were formed readily in wt-GlTIM and in the mutants C222A and C228A. The crystal structure of the dimer C202A mutant showed that the residues at position 202 of each monomer are in diametrically opposed locations (Figure 5(a)). Therefore, such topology allows the two C202 of the wt-GlTIM dimer to interact with the C202 of other dimers, and thus induce multimerization, as illustrated in Figure 5(b).

Intramonomeric disulfide bridge and activity control

We found that GlTIM has an intramonomeric disulfide bond between C222 and C228. It is relevant that catalysis is affected by this bond, indicating that there is a communication between this region and the catalytic site.

The addition of Cu^{2+} to the C202A mutant or the wild-type enzymes induced the loss of two Cys per subunit, and inactivation of the enzymes, through a process that was reversed by reducing agents. The activity of variants that lacked C222 or C228 was not modified by Cu^{2+}, even when they were in the tetra-

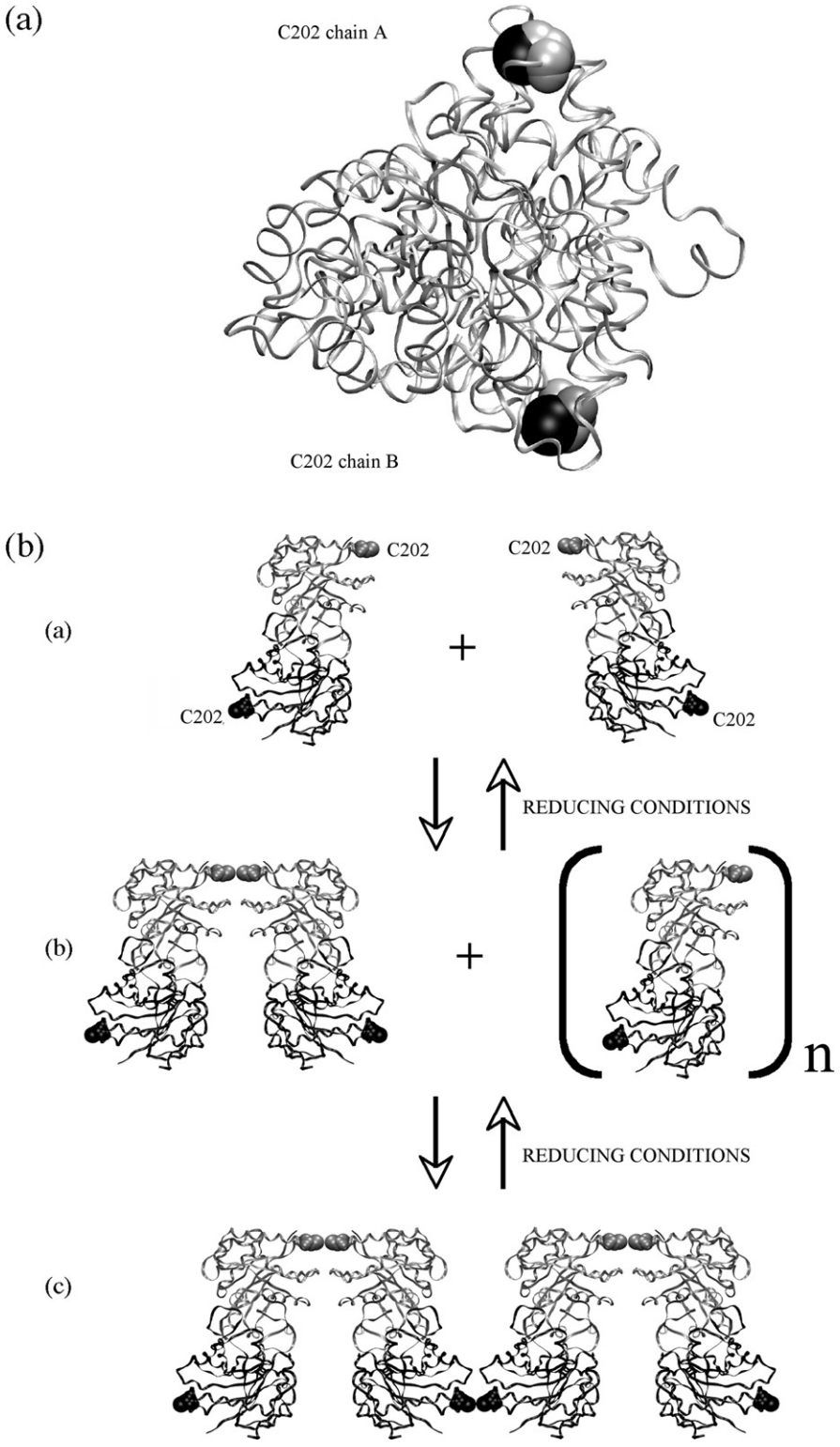

Figure 5. Topology of the residues C202 in the homodimeric GlTIM and their role in the oligomerization. (a) Top view of the homodimeric GlTIM. The C202 residues added *in silico* are shown as a CPK model. (b) A representation of the linking mechanism in homodimeric GlTIM. a, Side-view of two homodimers with their C202 aligned to form the disulfide bond. b, Upon disulfide formation, the tetramer produced can react with the C202 of another dimer. c, The reaction among several homodimers produces multimers of GlTIM; oligomerization can be reverted under reducing conditions. Figures were generated with VMD.[72]

meric state (see Table 1). This suggests that enzyme inactivation is due to the formation of the intramolecular disulfide bond, and not to oligomerization. Furthermore, the occupancy of the catalytic site by a ligand influences drastically the rate of formation of the intramonomeric bridge.

In reduced GlTIM there is a hydrogen bond between $N^{\delta 2}$ of N221 and the peptide oxygen atom of S216, which, in turn, is H-bonded to S174 and G178 (Figure 6(a)). When a disulfide bond is formed between C222 and C228, this H-bond network is disrupted (Figure 6(b)). S216 belongs to the highly conserved YGGS motif (residues 213–216 in loop 7) that interacts with loop 6 (residues 171–181) when it is in the closed conformation.[46,47] Molecular modeling of the C202A mutant with the disulfide bond formed between residues C222 and C228 showed that this bridge induces important structural rearrangements of loop 6 and helix 7. The C^{α} (S216) is displaced 4.6 Å from its original position, and the ϕ/φ value changes from (65°/24°) to (49.5°/76°). These modifications may perturb the conformational state that aligns the catalytic center with the substrate, and thereby diminishes the rate of catalysis.

It is known that the association of dimeric TIMs into higher oligomers, or with other proteins is a common phenomenon in hyperthermophiles, which apparently is related to their thermostability.[32,33,48,49] The oligomerization mediated by disulfide bridges is a peculiar property of GlTIM that apparently is not related to thermostability. Further studies are required to understand the metabolic role of high molecular mass oligomers in trophozoites and cysts.

Experimental Procedures

Trophozoites and cysts

Trophozoites of *G. lamblia* WB strain were cultured as described.[13] They were harvested in the log phase ($\approx 1\times10^6$ cells/ml) and induced to encyst by incubation at 37 °C for 24 h in TYI-S-33 medium with 5 mg/ml of bovine bile (a mixture of free and conjugated bile acids (SIGMA)) (pH 7.8) as described.[50] Cysts maturation was induced by incubation at 37 °C for 24 h in TYI-S-33 medium with 0.8 mg/ml of bovine bile (pH 7.2). Cysts were isolated by centrifugation in a discontinuous sucrose gradient (0.85 M and 1.5 M) at 690***g*** for 10 min at 4 °C. Cells were disrupted by sonication at 4 °C, five cycles of 20 s with 2 min of resting intervals in 50 mM Tris-HCl (pH 7.4), 1 mM phenylmethyl-sulfonyl fluoride, 1% (v/v) dimethyl sulfoxide. The sonicates were centrifuged at 15,700***g*** for 30 min at 4 °C, and the supernatants were withdrawn for analysis of soluble proteins.

Immunolocalization

Cells were fixed with 100% methanol for 5 min and 100% acetone for 2 min, at −20 °C.[51] Anti-GlTIM IgG was used at a concentration of 6 ng/ml. Anti-rabbit-IgG coupled to fluorescein isothiocyanate diluted 1:500 was used as the secondary antibody. Fluorescence microscopy was done with an Axiovert microscope (Zeiss).

Analysis and identification of GlTIM in trophozoites and cysts

Total proteins from cysts and trophozoites were analyzed by SDS-PAGE (12% (w/v) polyacrylamide gel) under non-reducing and reducing conditions,[13] and transferred to polyvinylidene difluoride membrane. Western blots were performed with 1.2 ng/ml of anti-GlTIM. Blot membranes were incubated with horseradish peroxidase-conjugated anti-rabbit IgG at 1:8000 (v/v) dilutions. Polyclonal antibodies against recombinant GlTIM were produced by immunization of rabbits. IgGs were purified from blood plasma using a protein A Sepharose column.

Immunoprecipitation of GlTIM

An aliquot of anti-GlTIM antibody (30 μg) was incubated with 2.5 mg of protein A Sepharose CL-4B (Pharmacia) at 4 °C for 16 h in 50 mM Tris–HCl (pH 7.0). After incubation, the protein A Sepharose was washed extensively with the Tris buffer. Soluble proteins from $\approx 7\times10^6$ trophozoites were immunoprecipitated with the complex formed between protein A Sepharose and anti-GlTIM at 4 °C for 2 h in 50 mM Tris–HCl (pH 7.0). The proteins that did not attach to anti-GlTIM were washed with the Tris buffer. The proteins bound to anti-GlTIM IgG were eluted using 200 μl of 0.1 M glycine (pH 2.7). The eluates were analyzed by SDS-PAGE and staining with Coomassie brilliant blue.

Wild-type GlTIM and mutants

Mutants C202A, C222A, and C228A were constructed by directed PCR mutagenesis.[39] Transformed *Escherichia coli* BL21(DE3)pLyS cells containing the *wt-gltim* or mutant genes were used to produce the recombinant enzymes. Purification was performed as described[13] with the additional use of anion-exchange (Q-Sepharose FF; 1.5 cm × 12 cm) and gel-filtration (Superdex 75 prep grade; 1.6 cm × 60 cm) chromatography. The protein concentrations of mutants and wt-GlTIM were calculated using the $\varepsilon_{280\ nm}$= 26,600 $M^{-1}cm^{-1}$.[52] To quantify total protein in extracts from trophozoites and cysts of *G. lamblia*, we used the bicinchoninic acid method with bovine serum albumin as standard.[53] The enzymes were stored under N_2 atmosphere, in order to prevent Cys oxidation.

Enzymatic activity assay

The activity of mutants and wt-GlTIM was assayed in the direction of GAP to DHAP, using a coupled system, by following the decay of NADH at 340 nm.[54] For the determination of kinetic constants, the concentration of GAP ranged from 0.1 mM to 3 mM. Kinetic parameters were calculated from initial velocities at each concentration of substrate. Cellular GlTIM activity was measured in the soluble fraction obtained from trophozoites and cysts. Specific activity is defined as the micromoles of substrate transformed per minute per milligram of protein. Measurements of the activity of each sample were made in duplicate, and each experiment was repeated at least three times.

Cysteine quantification

Cys residues were determined using Ellman's reagent under denaturing conditions.[55] The recombinant enzymes were added to a buffer containing 100 mM tricine (pH 8.5), 1 mM DTNB, 5% (w/v) SDS. The number of Cys residues per monomer was quantified following the increase of absorbance at 412 nm; $\varepsilon_{412\ nm}$ = 13.6 $mM^{-1}cm^{-1}$.

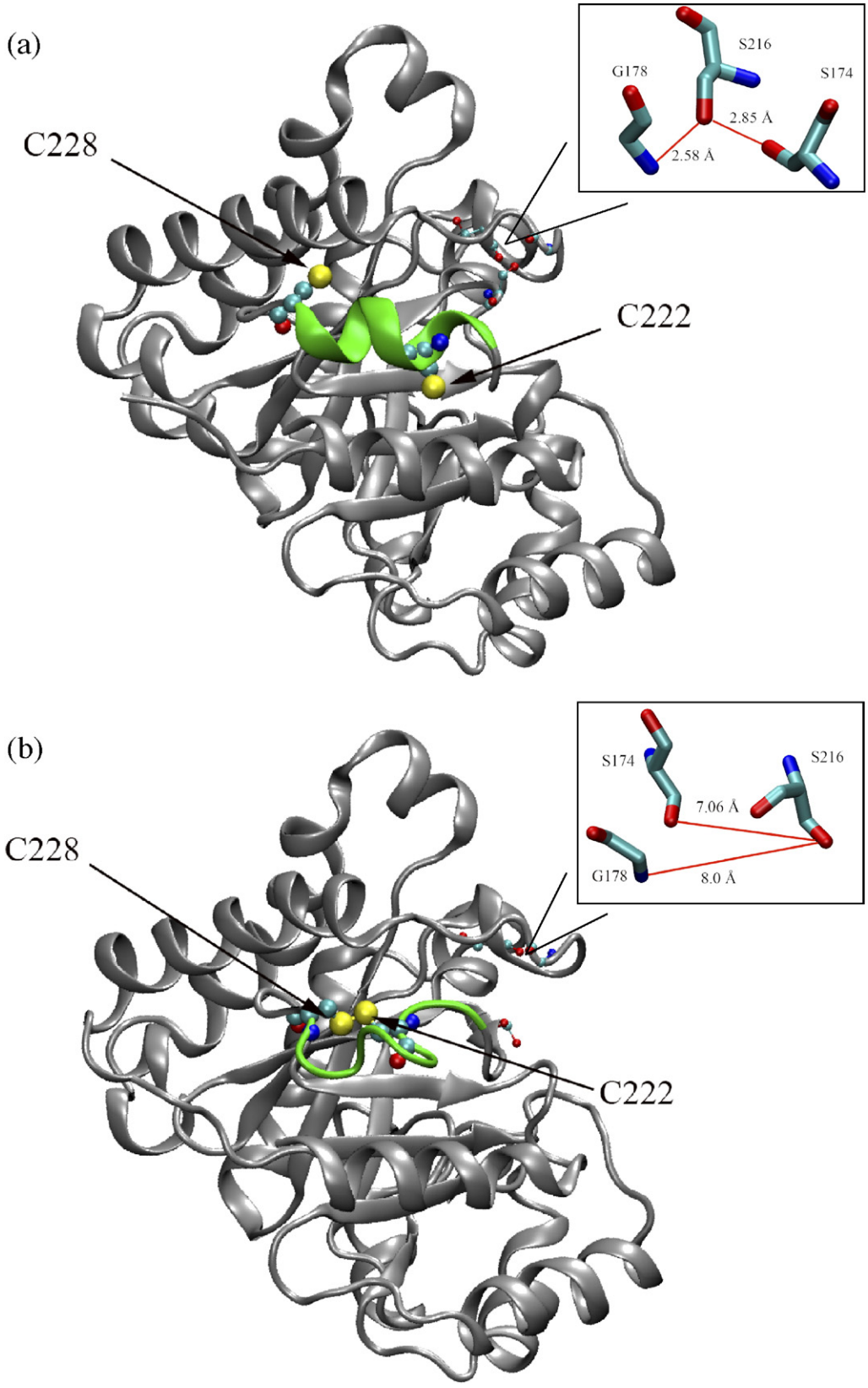

Figure 6. Structural changes induced by formation of a disulfide bond. (a) The C202A mutant from GlTIM without a disulfide bond (PDB code 2DP3). The inset shows hydrogen bonds among S174, S178 and G216. (b) A model constructed by molecular dynamics of the crystal structure exhibiting the disulfide bond between C222 and C228; the inset shows the breakage of the hydrogen bonds mentioned above. Green shows the changes in the secondary structure promoted by the disulfide bond formation (residues 221–228). Figures were generated with VMD.[72]

Crystallization and X-ray data collection

The enzyme was crystallized by the vapor-diffusion, sitting-drop method at 18 °C. Drops were formed with 5 μl of of C202A (13 mg/ml) dissolved in 100 mM triethanolamine (pH 7.4), 10 mM EDTA and mixed with 5 μl of 2 M ammonium sulfate, 5% (v/v) isopropanol. Orthorhombic crystals (space group *I*222) grew after two days. Diffraction data were collected at 113 K, using a single crystal and a Rigaku Raxis IIC image plate detector with a rotating anode generator. The cryoprotectant was 40% (w/v) trehalose. The data were processed and scaled with MOSFLM (CCP4).[56] The C202A structure was solved by molecular replacement with CNS,[57] using as starting model a composite structure based on 1TCD, 1LYX and 1M6J, performed by Swiss-model.[58–62], whereas model building and correction procedures were made with O[63] The refined model showed an *R*-factor of 17.5% and an R_{free} of 18.1%, with one monomer per asymmetric unit (Table 2). The GlTIM dimer was generated by the application of crystal symmetry operations. *In silico* substitution of A202 by Cys was performed to calculate its accessible surface area (ASA)†.[64] The relative ASA for this residue was 34% of the value for the same residue in the extended structure of the peptide Ala-Cys-Ala tripeptide.[65]

Table 2. Data collection and refinement statistics

A. *Data collection*	
Space group	*I*222
Unit cell dimensions	
a (Å)	55.37
b (Å)	100.44
c (Å)	118.79
Resolution range (Å)	15.0–2.1
Total reflections	49,262
Completeness (%)	94.1
Unique reflections	18,608
R_{merge} (%)	7.1
$\langle I/\sigma I \rangle$	8.9
B. *Refinement*	
Number of protein atoms	1938
Number of water molecules	305
Number of sulfate ions	20
R-factor (%)	17.5/
R-$_{free}$ (%)	18.1
rms deviation from ideal	
Bond lengths (Å)	0.004
Bond angles (deg.)	1.2
Torsion angles (deg.)	0.75
Mean *B*-factor	
Protein (Å^2)	11.5
Sulfate (Å^2)	40.8
Water (Å^2)	18.2

Model of GlTIM with an intramonomeric disulfide bond

We modeled the 3D structure of dimeric GlTIM with a disulfide bond between residues C222 and C228 of each of the two subunits. Disulfide bridges were defined after minor adjustments of the dihedral angle between the C^{α} and C^{β} from each of the two Cys. In this state, the distance between sulfur atoms was close to 10 Å. A realistic structure of GlTIM containing intrachain disulfide bonds was obtained through an energy minimization procedure followed by molecular dynamics simulations, using explicit solvent under constant temperature and pressure. The NAMD2 program and the CHARMM force field version 22 were employed,[66,67] considering the three sites point charge model TIP3P for the water molecules. Simulation of the equilibrium structure was performed by centering GlTIM in a pre-equilibrated box of water, maintaining a limit of at least 10 Å between the protein atoms and the box edges. Water molecules within 2.4 Å of a protein atom were removed. The full system was energy-minimized for 1000 steps before molecular dynamics simulation, followed by a gradual increase of temperature in 30 ps from 0 to 300 K in 25 K increments. Simulation was continued for 200 ps using a 1 fs integration step and considering periodic boundary conditions. Both high-frequency motions due to bond potentials of hydrogen and the internal geometry of water molecules were constrained by the SHAKE algorithm.[68] Langevin dynamics were used at 300 K with a damping coefficient of 5 ps^{-1}. A pressure of 1 atm (101,325 Pa) was maintained through a Langevin piston method with a period of 100 fs, and a damping time constant of 50 fs.[69] Electrostatic interactions were processed with the particle mesh Ewald summation method,[70] and a switching function was used for van der Waals interactions that ranged from 10 Å to 12 Å. The method produced a structure of GlTIM carrying the intramolecular disulfide with an interatomic distance between sulfur atoms of 2.01 Å. The structure was evaluated using PROCHECK,[71] showing 89.2% of the residues in the most favorable region, and 10.4% in the additionally allowed region of the Ramachandran plot.

Protein Data Bank accession number

The atomic coordinates and structure factors have been deposited in the Research Collaboratory for Structural Bioinformatics Protein Data Bank. The accession code ID is 2DP3.

† http://wolf.bms.umist.ac.uk/naccess/

Acknowledgements

Critical review of the manuscript by Dr Armando Gomez-Puyou and Dr Carlos Jimenez is acknowledged. We thank Carmen Ortiz and Reyna Lara-Martinez for technical assistance. This work was supported by grants from the Consejo Nacional de Ciencia y Tecnologia, Mexico (J37071-B to H.R.-V., and J43022-M to G.L.-V.). X-ray data were collected at the L.U.E.P., IQ, UNAM.

References

1. Eckman, L. (2003). Mucosal defences against Giardia. *Parasite Immunol.* **25**, 259–270.
2. Palm, D., Weiland, M., McArthur, A. G., Winiecka-Krusnell, J., Cipriano, M. J., Birkeland, S. R. *et al.* (2005). Developmental changes in the adhesive disk during Giardia differentiation. *Mol. Biochem. Parasitol.* **141**, 199–207.
3. Townson, S. M., Boreham, P. F. L., Upcroft, P. &

Upcroft, J. A. (1994). Resistance to the nitroheterocyclic drugs. *Acta Trop.* **56**, 173–194.
4. Upcroft, J. & Upcroft, P. (1998). My favorite cell: Giardia. *BioEssays*, **20**, 256–263.
5. Upcroft, J. & Upcroft, P. (1993). Drug resistance and Giardia. *Parasitol. Today*, **9**, 187–190.
6. Andrzejewska, M., Yépez-Mulia, L., Tapia, A., Cedillo-Rivera, R., Laudy, A. E., Starosciak, B. J. & Kazimierczuk, Z. (2004). Synthesis, and antiprotozoal and antibacterial activities of S-substituted 4,6-dibromo- and 4,6-dichloro-2-mercaptobenzimidazoles. *Eur. J. Pharm. Sci.* **21**, 323–329.
7. Schofield, P. J., Edwards, M. R. & Kranz, P. (1991). Glucose metabolism in Giardia intestinalis. *Mol. Biochem. Parasitol.* **45**, 39–48.
8. Tovar, J., León-Avila, G., Sánchez, L. B., Sutak, R., Tachezy, J., Van der Geizen, M. *et al.* (2003). Mitochondrial remnant organelles of Giardia function in iron-sulphur protein maturation. *Nature*, **426**, 172–176.
9. Gómez-Puyou, A., Saavedra-Lira, E., Becker, I., Zubillaga, R. A., Rojo-Dominguez, A. & Pérez-Montfort, R. (1995). Using evolutionary changes to achieve species-specific inhibition of enzyme action-studies with triosephosphate isomerase. *Chem. Biol.* **2**, 847–855.
10. Garza-Ramos, G., Cabrera, N., Saavedra-Lira, E., Tuena de Gómez-Puyou, M., Ostoa-Saloma, P., Pérez-Montfort, R. & Gómez-Puyou, A. (1998). Sulfhydryl reagent susceptibility in proteins with high sequence similarity. Triosephosphate isomerase from *Trypanosoma brucei*, *Trypanosoma cruzi* and *Leishmania mexicana*. *Eur. J. Biochem.* **253**, 684–691.
11. Rodríguez-Romero, A., Hernández-Santoyo, A., Del Pozo-Yauner, L., Kornhauser, A. & Fernández-Velasco, D. A. (2002). Structure and inactivation of triosephosphate isomerase from *Entamoeba histolytica*. *J. Mol. Biol.* **322**, 669–675.
12. Singh, S. K., Maithal, K., Balaram, H. & Balaram, P. (2001). Synthetic peptides as inactivators of multimeric enzymes: inhibition of *Plasmodium falciparum* triosephsophate isomerase by interface peptides. *FEBS Letters*, **501**, 19–23.
13. López-Velázquez, G., Molina-Ortiz, D., Cabrera, N., Hernández-Alcántara, G., Peon-Peralta, J., Yépez-Mulia, L. *et al.* (2004). An unusual triosephosphate isomerase from the early divergent eukaryote *Giardia lamblia*. *Proteins: Struct. Funct. Bioinform.* **55**, 824–834.
14. Albery, J. & Knowles, J. R. (1976). Evolution of enzyme function and the development of catalytic efficiency. *Biochemistry*, **64**, 5631–5640.
15. Albert, T., Banner, D. W., Bloomer, A. C., Petsko, G. A., Phillips, C., Rivers, P. S. & Wilson, I. A. (1981). On the three-dimensional structure and catalytic mechanism of triosephosphate isomerase. *Phil. Trans. Roy Soc. ser. B*, **293**, 159–171.
16. Nickbarg, E. B. & Knowles, J. R. (1988). Triosephosphate isomerase; energetics of the reaction catalyzed by the yeast enzyme expressed in *Escherichia coli*. *Biochemistry*, **27**, 5939–5947.
17. Knowles, J. R. (1991). Enzyme catalysis, not different, just better. *Nature*, **350**, 121–124.
18. Banner, D. W., Bloomer, A. C., Petsko, G. A., Phillips, D. C., Pogson, C. I., Wilson, I. A. *et al.* (1975). Structure of chicken muscle triosephosphate isomerase determined crystallographically at 2.5 Å resolution using aminoacid sequence data. *Nature*, **255**, 609–614.
19. Lolis, E., Albert, T., Davenport, R. C., Rose, D., Hartman, F. C. & Petsko, G. A. (1990). Structure of yeast triosephosphate isomerase at 1.9 Å resolution. *Biochemistry*, **29**, 6609–6618.
20. Wierenga, R. K., Noble, M. E. M., Vriend, G., Nauche, S. & Hol, W. G. J. (1991). Refined 1.83 Å structure of trypanosomal triosephosphate isomerase crystallized in the presence of 2.4 M-ammonium sulphate. A comparison with the structure of trypanosomal triosephosphate isomerase-glycerol-3-phosphate complex. *J. Mol. Biol.* **220**, 995–1015.
21. Noble, M. E. M., Zeelen, J. P., Wierenga, R. K., Mainfroid, V., Goraj, K., Gohimont, A. C. & Martial, J. A. (1993). Structure of triosephosphate isomerase from *Escherichia coli* determined at 2.6 Å resolution. *Acta Crystallog. sect. D*, **273**, 403–417.
22. Mande, S. C., Mainfoid, V., Kalk, K. H., Goraj, K., Martial, J. A. & Hol, W. G. (1994). Crystal structure of recombinant human triosephosphate isomerase at 2.8 Å resolution. Triosephosphate isomerase related human genetic disorders and comparison with the trypanosomal enzyme. *Protein Sci.* **3**, 810–821.
23. Delboni, L. F., Mande, S. C., Rentier-Delrue, F., Mainfroid, V., Turley, S., Vellieux, F. M. D. *et al.* (1995). Crystal structure of recombinant triosephosphate isomerase from *Bacillus stearothermophilus*. An analysis of potential thermostability factors in six isomerases with known three-dimensional structures points to the importance of hydrophobic interactions. *Proteins Sci.* **4**, 2594–2604.
24. Velanker, S. S., Ray, S. S., Gokhale, R. S., Suma, S., Balaram, H., Balaram, P. & Murphy, M. R. N. (1997). Triosephosphate isomerase from *Plasmodium falciparum*: the crystal structure provides insights into antimalarial drug design. *Structure*, **5**, 751–761.
25. Maldonado, E., Soriano-García, M., Moreno, A., Cabrera, N., Garza-Ramos, G., Tuena de Gómez-Puyou, M. & Gómez-Puyou, A. (1998). Differences in the intersubunit contacts in triosephosphate isomerase from two closely related pathogenic trypanosomes. *J. Mol. Biol.* **283**, 193–203.
26. Alvarez, M., Zeelen, J. P., Mainfroid, V., Rentier-Delrue, F., Martial, J. A., Wyns, L. *et al.* (1998). Triosephosphate isomerase (TIM) of the psychrophilic bacterium *Vibrio marinus*. Kinetic and structural properties. *J. Biol. Chem.* **273**, 2199–2206.
27. Maes, D., Zeelen, J. P., Thanki, N., Beaucamp, N., Alvarez, M., Dao Thi, M. H. *et al.* (1999). The crystal structure of triosephosphate isomerase (TIM) from *Thermotoga maritima*: a comparative thermostability structural analysis of ten different TIM structures. *Proteins: Struct. Funct. Genet.* **37**, 441–453.
28. Williams, J. C., Zeelen, J. P., Neubauer, G., Vried, G., Backmann, J., Michels, P. A. M. *et al.* (1999). Structural and mutagenesis studies of *Leishmania* triosephosphate isomerase: a point mutation can convert a mesophilic enzyme into a superstable enzyme without losing catalytic power. *Protein Eng.* **12**, 243–250.
29. Walden, H., Bell, G. S., Russell, R. J., Siebers, B., Hensel, R. & Taylor, G. L. (2001). Tiny TIM: a small, tetrameric, hyperthermostable triosephosphate isomerase. *J. Mol. Biol.* **306**, 745–757.
30. Aparicio, R., Ferreira, S. T. & Polikarpov, I. (2003). Closed conformation of the active site loop of rabbit muscle triosephosphate isomerase in the absence of substrate: evidence of conformational heterogeneity. *J. Mol. Biol.* **334**, 1023–1041.
31. Bell, G. S., Russell, R. J., Kohlhoff, H. M., Hensel, R., Danson, M. J., Hough, D. W. & Taylor, G. L. (1998). Preliminary crystallographic studies of triosephosphate isomerase (TIM) from the hyperthermophilic *Archaeon Pyrococcus woesei*. *Acta Crystallog. sect. D*, **54**, 1419–1421.

32. Kohlhoff, M., Dahm, A. & Hensel, R. (1996). Tetrameric triosephosphate isomerase from hyperthermophilic Archaea. *FEBS Letters*, **383**, 245–250.
33. Walden, H., Taylor, G., Lilie, H., Knura, T. & Hensel, R. (2004). Triosephosphate isomerase of the hyperthermophile *Thermoproteus tenax*: thermostability is not everything. *Biochem. Soc. Trans.* **32**, 305.
34. Brown, D. M., Upcroft, J. A. & Upcroft, P. (1993). Cysteine is the major low-molecular weight thiol in *Giardia duodenalis*. *Mol. Biochem. Parasitol.* **61**, 155–158.
35. Müller, S., Liebau, E., Walter, R. D. & Krauth-Siegel, R. L. (2003). Thiol-based redox metabolism of protozoan parasites. *Trends Parasitol.* **19**, 320–328.
36. Lujan, H. D. & Nash, T. E. (1994). The uptake and metabolism of cysteine by *Giardia lamblia* trophozoites. *J. Euk. Microbiol.* **41**, 169–175.
37. Noble, M. E., Zeelen, J. P. & Wierenga, R. K. (1993). Structures of the open and closed state of trypanosomal triosephosphate isomerase, as observed in a new crystal form: implications for the reaction mechanism. *Proteins: Struct. Funct. Genet.* **16**, 311–326.
38. Lolis, E. & Petsko, G. A. (1990). Crystallographic analysis of the complex between triosephosphate isomerase and 2-phosphoglycolate at 2.5 Å resolution. Implications for catalysis. *Biochemistry*, **29**, 6619–6625.
39. Hernández-Alcántara, G., Garza-Ramos, G., Mendoza-Hernandez, G., Gomez-Puyou, A. & Pérez-Montfort, R. (2002). Catalysis and stability of triosephosphate isomerase from *Trypanosoma brucei* with different residues at position 14 of the dimer interface. Characterization of a catalytically competent monomeric enzyme. *Biochemistry*, **41**, 4230–4238.
40. Sun, A. Q., Yüksel, K.Ü. & Gracy, R. W. (1992). Relationshicp between the catalytic center and the primary degradation site of triosephosphate isomerase: effects of active site modfication and deamidation. *Arch. Biochem. Bioqphys.* **293**, 382–390.
41. Maithal, K., Ravindra, G., Balaram, H. & Balaram, P. (2002). Inhibition of *Plasmodium falciparum* triosephosphate isomerase by chemical modification of an interface cysteine. *J. Biol. Chem.* **28**, 24114–25106.
42. Cecconi, I., Moroni, M., Vilardo, P. G., Dal Monte, M., Borella, P., Rastelli, G. *et al.* (1998). Oxidative modification of aldose reductase induced by copper ion. Factors and conditions affecting the process. *Biochemistry*, **37**, 14167–14174.
43. Cecconi, I., Scaloni, A., Rastelli, G., Moroni, M., Vilardo, P. G., Costantino, L. *et al.* (2002). Oxidative modification of aldose reductase induced by copper ion. Definition of the metal-protein interaction mechanism. *J. Biol. Chem.* **277**, 42017–42027.
44. Schliebs, W., Thanki, N., Eritja, R. & Wierenga, R. K. (1996). Active site properties of monomeric triosephosphate isomerase (monoTIM) as deduced from mutational and structural studies. *Protein Sci.* **5**, 229–239.
45. Ladokhin, A. S. (2000). Fluorescence spectroscopy in peptide and protein analysis. In *Encyclopedia of Analytical Chemistry* (Meyers, R. A., ed), pp. 5762–5779, John Wiley and Sons Ltd, Chichester, UK.
46. Sampson, N. S. & Knowles, J. R. (1992). Segmental movement: definition of the structural requirements for loop closure in catalysis by triosephosphate isomerase. *Biochemistry*, **31**, 8488–8494.
47. Kursula, I., Salin, M., Sun, J., Norledge, B. V., Haapalainen, A. M., Sampson, N. S. & Wierenga, R. K. (2004). Understanding protein lids: structural analysis of active hinge mutants in triosephosphate isomerase. *Protein Eng. Des. Select.* **17**, 375–382.
48. Yu, J. S. & Noll, K. M. (1995). The hyperthermophilic bacterium *Thermotoga neapolitana* possesses two isozymes of the 3-phosphoglycerate kinase/triosephosphate isomerase fusion proteins. *FEMS Microbiol. Letters*, **131**, 307–312.
49. Beaucamp, N., Hofmann, A., Kellerer, B. & Jaenicke, R. (1997). Dissection of the gene of the bifunctional PGK-TIM fusion protein from the hyperthermophilic bacterium *Thermotoga maritima*: design and characterization of the separate triosephosphate isomerase. *Protein Sci.* **6**, 2159–2165.
50. Arguello-García, R., Arguello-López, C., González-Robles, A., Castillo-Figueroa, A. M. & Ortega-Pierres, M. G. (2002). Sequential exposure and assembly of cyst wall filaments on the surface of encysting *Giardia duodenalis*. *Parasitology*, **125**, 209–219.
51. Spector, D. L. & Smith, H. C. (1986). Redistribution of U-snRNPs during mitosis. *Expt. Cell Res.* **163**, 87–94.
52. Pace, C. N., Vajdos, F., Fee, L., Grimsley, G. & Gray, V. (1995). How to measure and predict the molar absorption coefficient of a protein. *Protein Sci.* **4**, 2411–2423.
53. Smith, P. K., Krohn, R. I., Hermanson, G. T., Mallian, A. K., Gartner, F. H., Provezano, M. D. *et al.* (1985). Measurement of protein using bicinchoninic acid. *Anal. Biochem.* **150**, 76–85.
54. Garza-Ramos, G., Pérez-Montfort, R., Rojo-Domínguez, A., Tuena de Gómez-Puyou, M. & Gómez-Puyou, A. (1996). Species-specific inhibition of homologous enzymes by modification of nonconserved amino acids residues. The cysteine residues of triosephosphate isomerase. *Eur. J. Biochem.* **241**, 114–120.
55. Ellman, G. L. (1958). A colorimetric method for determining low concentrations of mercaptans. *Arch. Biochem. Biophys.* **74**, 443–450.
56. Collaborative Computational Project, Number 4. (1994). The CCP4 suite: programs for protein crystallography. *Acta Crystallog. sect. D*, **50**, 760–763.
57. Rossman, M. G. & Blow, D. M. (1962). The detection of sub-units within the crystallographic asymmetric unit. *Acta Crystallog. sect. A*, **15**, 24–31.
58. Peitsch, M. C. (1995). Protein modelling by E-Mail. *Bio/Technology*, **13**, 658–660.
59. Guex, N. & Peitsch, M. C. (1997). SWISS-MODEL and the Swiss-PdbViewer: an environment for comparative protein modeling. *Electrophoresis*, **18**, 2714–2723.
60. Schwede, T., Kopp, J., Guex, N. & Peitsch, M. C. (2003). SWISS-MODEL: an automated protein homology-modeling server. *Nucl. Acid Res.* **31**, 3381–3385.
61. Brünger, A. T. (1992). The free R value: a novel statistical quantity for assessing the accuracy of crystal structures. *Nature*, **355**, 472–474.
62. Brünger, A. T., Adams, P. D., Clore, G. M., Delano, W. L., Gros, P., Grosse-Kuntsleve, R. W. *et al.* (1998). Crystallography and NMR system: a new software suite for macromolecular structure determination. *Acta Crystallog. sect. D*, **54**, 905–921.
63. Jones, T. A., Zou, J. Y., Cowan, S. W. & Kjeldgaard, M. (1991). Improved methods for building protein models in electron density maps and the location of errors in these models. *Acta Crystallog. sect. A*, **47**, 110–119.
64. Gerstein, M. (1992). A resolution-sensitive procedure for comparing protein surfaces and its application to the comparison of antigen-combining sites. *Acta Crystallog. sect. A*, **48**, 271–276.
65. Hubbard, S. J., Campbell, S. F. & Thornton, J. M. (1991). Molecular recognition. Conformational analysis of limited proteolytic sites and serine proteinase protein inhibitors. *J. Mol. Biol.* **220**, 507–530.
66. Kalé, L., Skeel, R., Bhandarkar, M., Brunner, R.,

Gursoy, A., Krawetz, N. *et al.* (1999). NAMD2: greater scalability for parallel molecular dynamics. *J. Comput. Phys.* **151**, 283–312.
67. MacKerell, A. D., Jr, Bashford, D., Bellott, M., Dunbrack, R. L., Jr., Evanseck, J. D., Field, M. J. *et al.* (1998). All-atom empirical potential for molecular modeling and dynamics studies of proteins. *J. Phys. Chem. B*, **102**, 3586–3616.
68. Van Gunsteren, W. F. & Berendsen, H. J. C. (1977). Algorithms for macromolecular dynamics and constraint dynamics. *Mol. Phys.* **34**, 1311–1327.
69. Feller, S. E., Zhang, Y. H., Pastor, R. W. & Brooks, B. R. (1995). Constant pressure molecular dynamics simulation: the Langevin piston method. *J. Chem. Phys.* **103**, 4613–4621.
70. Darden, T., York, D. & Pedersen, L. (1993). Particle mesh Ewald: an N·log(N) method for Ewald sums in large systems. *J. Chem. Phys.* **98**, 10089–10092.
71. Laskowski, R. A., MacArthur, M. W., Moss, D. S. & Thornton, J. M. (1993). PROCHECK: a program to check the stereochemical quality of protein structures. *J. Appl. Crystallog.* **26**, 283–291.
72. Humphrey, W., Dalke, A. & Schulten, K. (1996). VMD: visual molecular dynamics. *J. Mol. Graph.* **14**, 33–38.

Edited by M. Guss

(Received 20 July 2006; received in revised form 12 October 2006; accepted 17 October 2006)
Available online 21 October 2006